Fibers and Polymers 2018, Vol.19, No.9, 1930-1939
DOI 10.1007/s12221-018-8227-7

ISSN 1229-9197 (print version)
ISSN 1875-0052 (electronic version)

Synthesis of Ag-Loaded TiO_2 Electrospun Nanofibers for Photocatalytic Decolorization of Methylene Blue

M. Raffi[1]*, Zaira Batool[2], Mashkoor Ahmad[3], M. Zakria[1], Rana I. Shakoor[4], Muhammad Aslam Mirza[2], and Arshad Mahmood[1]

[1]*Department of Materials Engineering, National Institute of Lasers and Optronics (NILOP), Islamabad-45650, Pakistan*
[2]*Department of Chemistry, Mirpur University of Science and Technology (MUST), Mirpur-10250 (AJK), Pakistan*
[3]*Nanomaterials Research Group, Pakistan Institute of Nuclear Science and Technology (PINSTECH), Islamabad 45650, Pakistan*
[4]*Department of Mechatronics Engineering, Air University, Sector E-9, Islamabad 44000, Pakistan*
(Received April 1, 2018; Revised June 15, 2018; Accepted July 2, 2018)

Abstract: Titanium dioxide (TiO_2) is one of the excellent photocatalysts used for degradation of environmetal pollutants. In this work, 2.5, 5.0 and 7.5 wt.% of silver (Ag)-loaded TiO_2 nanofibers of mean size 52-134 nm were synthesized by electrospinning method. These electrospun nanofibers were calcined at 500 °C to enable the transformation of Rutile (R) phase to Anatase (A), elimination of reaction moieties from the TiO_2 matrix and subsequently formation of Ag clusters. The effect of Ag loading on the morphology, crystal structure, phase transformation, and band gap of these electrospun nanofibers have been characterized by scannining electron microscopy (SEM), X-ray diffraction (XRD), fourier transform infrared spectroscopy (FTIR), raman spectroscopy and UV-visible spectroscopy. These nanofibers exhibited a red-shift in the absorbance edge and a significant enhancement of light absorption in the wavelength range of 250-550 nm. These electrospun nanofibers were investigated for photodecomposition of methylene blue (MB), and photocatalytic decolorization rates were determined by pseudo-first-order equation. The rate constants for the pure and those of 2.5, 5.0, and 7.5 wt% Ag-loaded TiO_2 nanofibers were computed to be 0.1439 min^{-1}, 0.1608 min^{-1}, 0.1876 min^{-1}, and 0.2251 min^{-1} respectively.

Keywords: Nanofibers, TiO_2, Crystal structure, Photocatalysis, Degradation, Electron microscopy

Introduction

Photocatalytic oxidation has widely been investigated to propose solutions to a variety of environmental pollution problems especially water treatment processes [1]. Cationic dyes are considered harmful for their non biodegradability, toxicity, accumulation in the living organisms, and related hazards at higher concentrations. Methylene blue (MB) is a cationic dye, which is water soluble having extensive industrial applications such as dyeing and printing of textile, leather, calico and cotton, and in the biological staining processes [2]. MB has carcinogenic effects and causes various diseases such as allergic dermatitis, skin irritation, dysfunction of kidney, liver, brain, reproductive, and central nervous system [3]. Significantly successful treatment methods for the removal of dyes from industrial effluents include adsorption, bioremediation, photocatalysis [4], fenton chemical oxidation, electrochemical degradation, cation exchange membranes, and flocculation coagulation [5] but novel techniques based on green chemistry are being investigated to propose solutions to the environmental challenges. Among the several semiconductors, titanium dioxide (TiO_2) is considered an efficient and environmentally benign photocatalyst. It has been used extensively for photodegradation of multiple pollutants and is belived to play a vital role in solving key environmental challenges due to its relatively high oxidative power, photostability, nontoxicity, chemical stability, large surface area and low production cost [6]. It is widely used in many applications such as photocatalysis, bio-sensing, photovoltaics, dye-sensitized solar cells, photonic crystals [7] and possesses, and tailoring self-cleaning and self-healing characteristics [8]. TiO_2 exists in three crystalline phases; anatase (A), rutile (R), and brookite (B) but most common crystalline polymorphs of TiO_2 are metastable A and stable R-phases. The presence of either or both of these crystalline phases impacts the photocatalytic performance of TiO_2 [9]. A-phase has been reported to have a lower surface enthalpy and surface free energy than R-phase. Hence, it is expected that the wetting of A-phase by water would be less than that of R-phase since higher surface free energies generally contribute to hydrophilicity. The photocatalytic activity of A and R-phases has been investigated, explored and interpreted by Sclafani and Herrmann with reference to the densities of surface-adsorbed species [10]. Their study has reported that higher levels of radicals adsorbed on the A-surface give rise to the significantly favorable photoactivity than R. Photocatalytic reactions are believed to take place primarily on the surface of the catalyst, eventully, the redox energies and adsorption characteristics at the catalyst/solution interfaces, both play critical role in the photochemical reactions [11]. For the development of highly selective photocatalyst, it is much easier to modify the adsorption characteristics than to change the redox energies. Usually, the preferentially adsorbed

*Corresponding author: muhammad_raffi@hotmail.com

pollutants can react more efficiently with the active radicals, thus selective photocatalytic activities on these pollutants can be observed [12]. Certain applications of TiO_2 are associated to the A-phase, which exhibit a relatively large energy band gap (~3.2 ev) attained only by UV irradiation using wavelength smaller than 388 nm. This characteristic is a limitation for applications, because fast recombination of electron-hole pair produced by the photon excitation reduces its photostability, consequently lowering the catalytic efficiency [13].

Modification of electronic band structure of TiO_2 by various procedures, such as coupling with narrow band gap semiconductor, metal/non-metal ion doping [14], surface sensitization by organic dyes or metal complexes [15], noble metal deposition and co-doping with two or more foreign ions, is one of the strategies to overcome the large band gap of TiO_2. On the other hand, noble metal nanoparticles store electrons and act as sink for the interfacial charge transfer processes [16]. However, some noble metals such as Pt, Pd, Rh, and Au are too expensive to be used at industrial scale. Thus, research on development of Ag loaded TiO_2 structures has a significant practical value. The surface plasmon resonance (SPR) of Ag nanoparticles dispersing onto the surface of TiO_2 increases with Ag contents. Subsequently, this increase in SPR can enhance electric fields, which assists electron-hole production resulting into increased absorption in the visible range [17]. Recently, researchers have reported superior results employing a convenient, cost effective and efficacious method by using oxidized biopolymer layers for immobilization of TiO_2 powder for applications to separate pollutants from the waste water [18,19]. Several desirable characteristics such as surface area to volume ratio, flexibility in surface functionalities and superior mechanical properties can be achieved, when diameter of TiO_2 is reduced to the nanoscale. So far, many methods including sol gel, hydrothermal, electrospinning, melt blowing, phase separation, self-assembly and template synthesis, have been developed to synthesize TiO_2, nanomaterials, such as nanoparticles, nanofilms, nanotubes, and nanofibers. However, electrospinning process is deemed technically sound, environment friendly, cost-effective and viable method for synthesizing TiO_2 nanofibers at room temperature and pressure [20,21].

In this research work, pristine and Ag-loaded TiO_2 electrospun nanofibers have been synthesized to suppress the electron-hole recombination and revamping of crystalline phases as a function of Ag-loading and calcination. These pristine and Ag-loaded TiO_2 nanofibers samples have been characterized by SEM, XRD, FT-IR, Raman Spectroscopy (RS) to evaluate their morphology and structure. Furthermore, the effect of Ag-loading on the optical phonon modes, mean size, crystallite growth, and photocatalytic performance of these nanofibers have been determined. Finally, the efficacy of pristine and Ag-loaded TiO_2 nanofibers has been investigated for the photocatalytic decolorization of methylene blue (MB) under the exposure of UV-light.

Experimental

Synthesis of Nanofibers

All materials, which include poly vinylpyrolidone (PVP; MW=1,300,000, 98 %) titanium isopropoxide (TIP; MW= 284.26, 98 %), ethanol (94-96 %), silver nitrate (99.9 %) of Sigma-Aldrich, whereas acetic acid (99.7 %) of Alfa Aesar, have been used as-purchased from the vendors to synthesize pristine and Ag-loaded TiO_2 nanofibers. The prepared solution was filled into a 1 m*l* disposable plastic syringe equipped with 23 gauge stainless steel (SS) needle which was fixed on the syringe pump. The details of solution preparation procedure have been given in the previous published work [17]. The positive terminal of high-voltage DC power supply (50 kV, DEL Electronic Corporation, USA) fixed at 18 kV (dc) has been connected to the SS needle, while the circular copper collector plate wraped in aluminum foil was grounded. The distance between needle tip and collector plate was kept 12 cm. The solution effused at a controlled rate from the needle was electrospun at ambient temperature and pressure to synthesize nanofibers. These samples were calcinated at a heating rate of 5 $^oC\text{-}min^{-1}$ in the box furnace (KSL-1200X-J, USA) at 500 ^oC for 3 h to remove PVP and other moieties. All of these TiO_2 nanofibers, pristine and Ag-loaded with a range of weight percentages (0.0, 2.5, 5.0 and 7.5 wt% of Ag with respect to TIP), were synthesized keeping the same experimental conditions. The morphology of these nanofibers was observed by the scanning electron microscope (SEM) (FORMAT JEOL/EO, version 1.1). The crystalline structure and phase transformation in these nanofibers have been evaluated by X-ray diffraction analysis performed in the 2θ range of 20 ^{o} to 90 ^{o} by using diffractometer (Bruker D-8 Discover HR-XRD) equipped with CuK_α (λ=1.5418 Å) X-ray radiation source. Fourier transform infrared (FTIR) spectroscopic analysis was carried out on the samples by using FTIR-ATR spectrometer (Thermo Nicolet 6700) in the spectral range 4000-400 cm^{-1} at a resolution of 6 cm^{-1}. Raman spectra were recorded on the spectrometer (DongWoo Optron MST-4000A, Korea) equipped with a 532 nm laser excitation source. While performing Raman analysis on the samples, exposure time was maintained to 7 sec, number of accumulations were 5 whereas laser power was fixed at 20 mW. UV vis absorption wavelength of ethanol suspensions (2 mg/4 m*l*) of pristine and Ag-loaded TiO_2 nanofibers were measured by UV-visible spectrophotometer (Perkin Elmer Lambda 950) in the wavelength range 250-550 nm. These absorption wavelengths were used to compute the band gap energies of pristine and Ag-loaded TiO_2 nanofibers.

Photocatalytic Activity of Electrospun Nanofibers

To study the photocatalytic efficacy of calcined pristine as

well as 2.5, 5.0 and 7.5 wt% Ag-loaded TiO_2 nanofibers, 25 mg of each type of nanofiber sample was added into 50 m*l* of the aqueous methylene blue (10 mg/*l*, 98 %, Sigma-Aldrich) solutions respectively. The reaction mixtures (pH 6.3) were kept in the dark for 30 min to allow the equilibration under continuous magnetic stirring on hot-plate at room temperature. After an interval of 30 min, these reaction mixtures were exposed to the UV radiations (λ=365 nm) using a UV-lamp (Xenon, 300 W) under continuous stirring condition. Ten samples from this reaction mixture were periodically collected in 5 m*l* aliquots after an interval of every 2 min. These samples were then centrifuged at 5000 rpm to remove the catalyst and UV-visible absorption measurements were carried out on supernatant using UV-visible spectrophotometer (Perkin Elmer Lambda 950) in the wavelngth range 400-800 nm. From the absorbance measured at λ=664 nm, the corresponding dye concentrations were calculated using the calibration curve. The decolorization rate (k) constant and decolorization efficiency were calculated by using pseudo-first-order equation (equation (1)), and Langmuir-Hinshelwood equation (2) [22]

$$\ln\left(\frac{C_0}{C}\right) = k'Kt = kt \tag{1}$$

$$r = \frac{dC}{dt} = \frac{kKC}{1+KC} \tag{2}$$

where r is the rate of decolorization (mgl^{-1}min), C_0 is the initial concentration of the MB (mgl^{-1}), C is the concentration of the MB (mgl^{-1}), t is the illumination time (min), k is the decolorization rate constant (min^{-1}), and K is the adsorption coefficient ($l$mg^{-1}). The photocatalytic efficiency was calculated using the following equation (3) [23].

$$\text{MB colour removal (\%)} = \left(\frac{C_0 - C_t}{C_0}\right) \times 100 \tag{3}$$

These experiments were performed to observe the photocatalytic efficiency of the nanofibers against MB.

Results and Discussion

SEM Analysis

The SEM micrographs of calcined nanofibers, pristine and Ag-loaded TiO_2, are given in Figure 1. From these micrographs, it has been noticed that the extent of roughness on the outer surfaces of nanofibers has increased with the rising Ag-loading. It is believed that with the increase of Ag-content, Ag-nanoparticles have formed on the outer surfaces of the nanofibers [17,24]. As the relative ratio of weight percentages of Ag-TiO_2 has increased gradually, which facilitated extensive coverage of TiO_2 nanofibers with the Ag nanoparticles, as shown in Figure 1(I-IV). The deposition of Ag-nanoparticles on the surfaces of nanofibers has also been supported by the XRD analysis, which is shown in

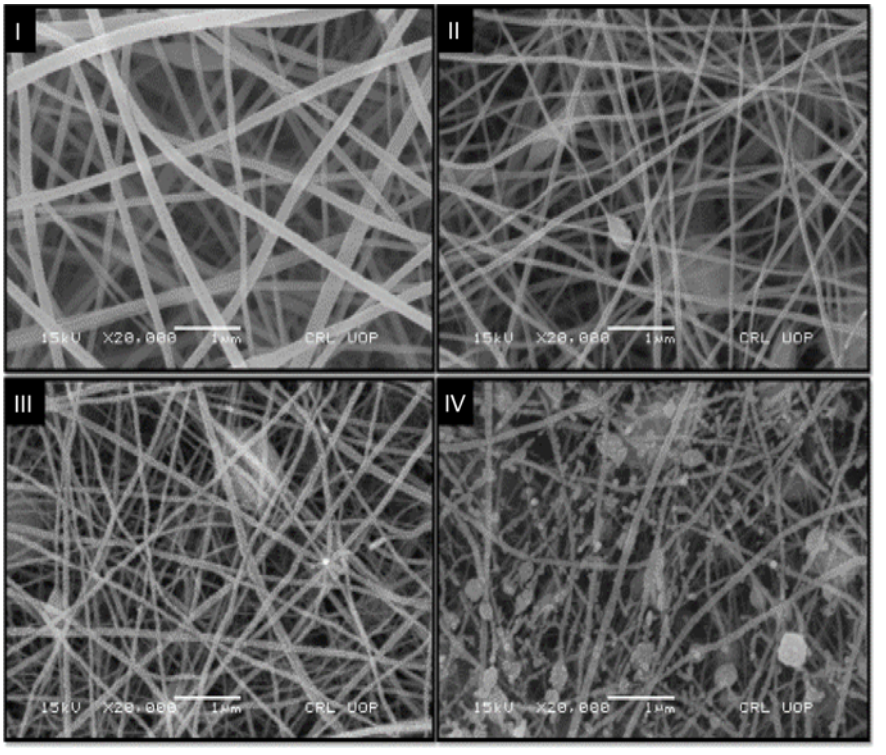

Figure 1. SEM micrographs of electrospun nanofibers calcined at 500 °C; (I) pristine TiO_2, (II) 2.5 wt% (III) 5.0 wt%, and (IV) 7.5 wt% Ag-loaded TiO_2.

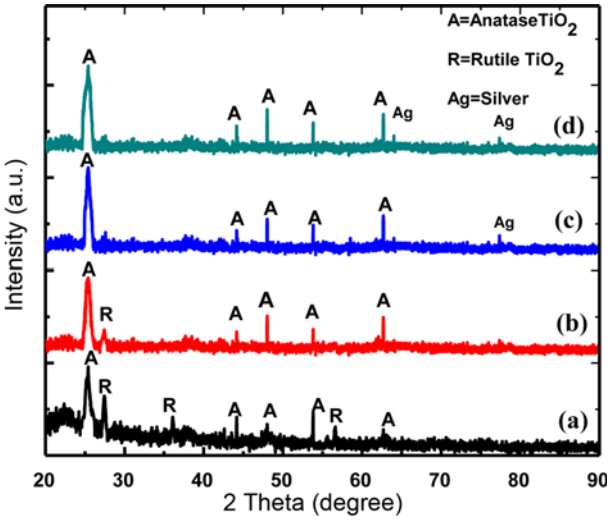

Figure 2. XRD diffraction patterns of electrospun nanofibers calcined at 500 °C; (a) pristine TiO_2, (b) 2.5 wt%, (c) 5.0 wt%, and (d) 7.5 wt% Ag-loaded TiO_2.

Figure 2. This characteristic lead to have a positive effect on the photocatalysis due to the enhancement of active surfaces [25]. An interesting feature observed in these SEM micrographs is the formation of 1D nanostructure in the nanofibers which remained stable even at higher Ag-loadings.

XRD Analysis

The crystalline phases of heat treated nanofiber samples were investigated by the XRD analysis. Diffraction patterns of pristine and Ag-loaded TiO_2 nanofibers are given in Figure 2. Both A and R-phases have been observed in the pristine TiO_2 nanofibers, while those loaded with Ag have only the A- phase. The diffraction peaks appeared at 25.40 °, 48.02 °, 53.82 °, 44.16 ° and 62.70 ° corresponded well to the (101), (200), (105), (211) and (204) crystalline planes of the A-phase, while peaks observed at 27.45 °, 36.09 ° and 56.64 ° were associated to (110), (101) and (220) (pdf No. 01-083-2243) planes and attributed to R-phase respectively [17,26]. The diffraction peaks noticed at 64.02 ° and 77.36 °° corresponded to (220) and (311) planes (pdf No. 01-071-4612) which represented the Ag. Both A and R-phases have been observed in pristine TiO_2 nanofibers. While the samples loaded with Ag have exhibited a gradual diminishing trend for the R-phase with the rise in Ag loading, as a result have exhibited A-phase in case of highest Ag content. It is believed that surface defect density in the Ag-loaded nanofibers has increased with the Ag content which supported the phase transformation because such type of defects were considered nucleation sites for the growth of R-phase. Additionally, surface oxygen vacancy concentration of A-phase grains increased with Ag-loading which favored the rearrangement of ions and reorganization of the structure for R-phase [17, 27]. Another possible reason may be that the domain mobility which is restricted due to the pinning of domain boundaries by the presence of crystal defects [28]. Dopants that do not dissolve and remain at the grain boundaries restrict the grain growth and reduce interparticle contact, thereby inhibiting the phase transformation [29,30]. Thus, Ag dopant retrained the anatase to rutile phase transformation.

FT-IR Analysis

FT-IR analysis has been performed on the samples in the spectral range 4000 to 400 cm^{-1} to examine the chemical composition, purity and bonding features of calcined nanofibers, as shown in the Figure 3. The peak observed at 650 cm^{-1} corresponded to the Ti-O bond in calcined nanofibers samples, which strongly supported the formation of TiO_2 nanostructures [31]. The absorption intensity at 650 cm^{-1} has been observed to be shifted towards the lower wave numbers with the rise in the Ag contents, demonstrating formation of Ag-TiO_2 nanocomposite system [29]. A red shift in the absorption has been observed in the Ag-loaded TiO_2 nanofibers displayed formation of metal clusters which give rise to the localized energy in the band gap, furthermore believed to have taken place due to the surface plasmon resonance (SPR) owing to the presence of Ag nanoparticles [32]. This behavior has been observed prominently in the nanofibers with higher weight percent Ag (7.5 wt%) loading, which have shown relatively substantial red-shift. Moreover, the red-shift noticed from 650 cm^{-1} to 450 cm^{-1} in the peak of Ti-O stretching mode has demonstrated the rearrangement in the crystal structure of TiO_2 from R to A-phase upon calcination [17].

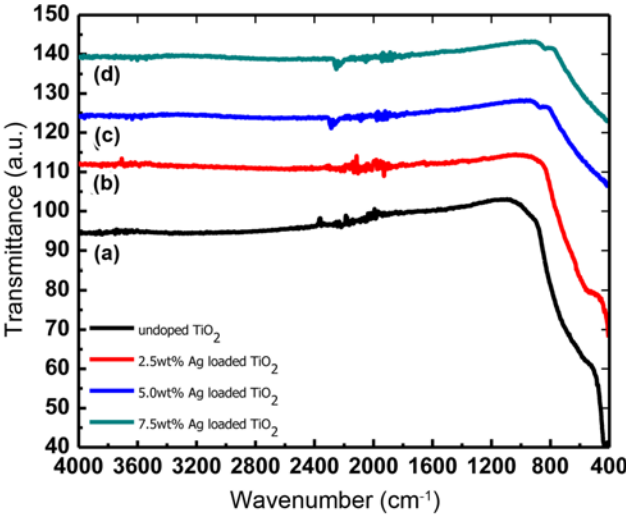

Figure 3. FT-IR spectra of electrospun nanofibers calcined at 500 °C of (i) pristine TiO_2, (ii) 2.5 wt%, (iii) 5.0 wt%, and (iv) 7.5 wt% Ag-loaded TiO_2.

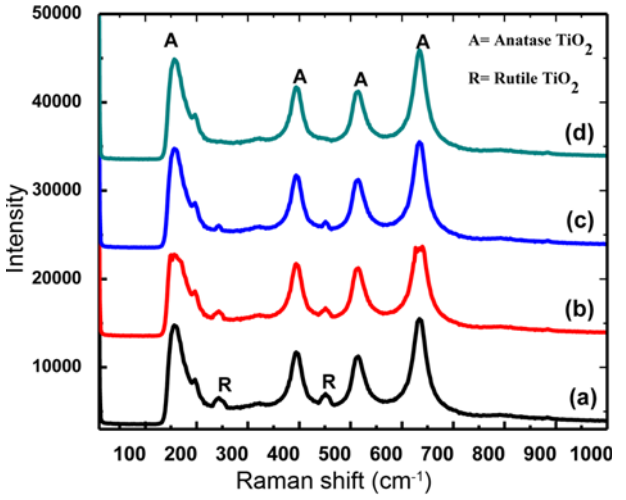

Figure 4. Raman spectra of electrospun nanofibers calcined at 500 °C of (a) pristine TiO_2, (b) 2.5 wt%, (c) 5.0 wt%, and (d) 7.5 wt% Ag-loaded TiO_2.

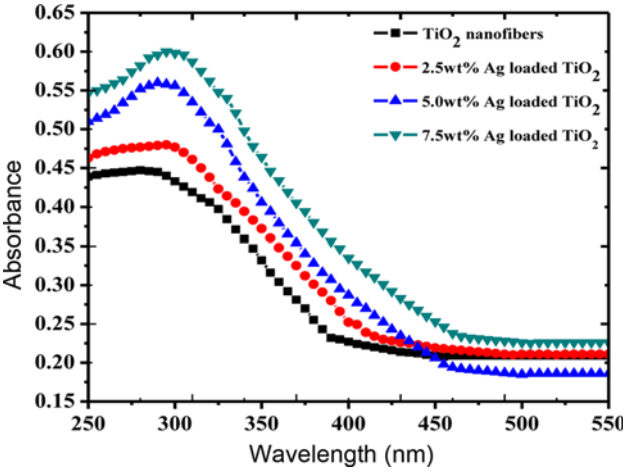

Figure 5. UV-vis absorption spectra of Ag-loaded TiO_2 nanofibers calcined at 500 °C.

Raman Spectroscopy

Raman Spectroscopy (RS) is considered distinctly an effective technique used to investigate the local and dynamic crystal structure symmetries in the materials. The transfotmation of R to A-phase in the crystalline structure of TiO_2 electrospun nanofibers has been observed by raman spectroscopy as a function of Ag loading in the matrix. Figure 4 shows the prominent Raman peaks observed in the calcined samples which have clearly illustrated the existence of crystallinity. The four raman vibration bands observed at 156(E_g), 393(B_{1g}), 514(A_{1g}) and 635(E_g) cm^{-1} respectively have been ascribed to A, whereas 244 (E_g), and 450 (A_{1g}) cm^{-1} illustrated the R-phase structures ranging between 100 and 1000 cm^{-1} [29,30]. Here, the two raman bands observed at 156 cm^{-1} and 393 cm^{-1} are attributed to the O-Ti-O bending-type vibrations, while the other two modes having peaks at 514 cm^{-1} and 635 cm^{-1} attributed to Ti-O bond stretching-type vibrations [17,33]. A small peak (knee) observed at 196.5 cm^{-1} (E_g) has been assigned to A-phase of TiO_2 [34]. The intensities of two relatively small R-phase peaks have been noted to be receding with the rising Ag content in the TiO_2 matrix, whereas the crystalline phase have been found transformed to A-phase at 7.5 wt% Ag loading.

UV-Visible Absorption Spectroscopy

The energy difference between the top of the valence band to the bottom of the conduction band is known as energy band gap. The electrons are able to jump from the valence to conduction band by absorption of specific amount of energy, known as the band gap energy [35]. The absorption wavelength of pristine and Ag-loaded TiO_2 nanofibers were measured by UV-visible absorption spectrophotometer in the wavelngth range 200-800 nm. Figure 5 shows the UV-vis absorption spectra of the 0.0, 2.5, 5.0 and 7.5 wt% Ag-loaded TiO_2 nanofibers. Band gap energies were calculated using the following relationship of photon energy and frequency (c/λ):

$$E = hc/\lambda \quad (4)$$

where h is Planck's constant (6.63×10^{-34} Js), c is the speed of light (2.99×10^{8} m/s) and λ is the wavelength of light [36]. As shown in Figure 6, the cut off wavelength was determined by extrapolation of base line and absorption edge to calculate energy band gap. The cut off wavelength (nm) and calculated energy band gap (eV) of pristine and Ag-loaded TiO_2 nanofibers are given in Table 1. The band gap of Ag-loaded TiO_2 nanofibers has been found reduced due to the SPR of Ag nanoparticles present there. The Ag-loaded nanofibers have exhibited an obvious red-shift in absorbance edge and a significant enhancement of light absorption in the region of 250-550 nm. Since the Fermi level of Ag is lower than that of TiO_2, therefore Ag nanoparticles adsorbed on the surface of the nanofibers acted as intermediate agents for the transfer of photo-induced electrons from the valence band of TiO_2 to an acceptor (O_2 gas) [37]. Therefore, Ag can enhance the photo-induced electron-hole separation and constrain their recombination resulting in increased absorption of visible light. It has been assessed that absorption in the visible range in Ag loaded nanofibers has proportionally increased with the Ag content. The SPR of Ag nanoparticles dispersing onto the surface of TiO_2 nanofibers has intensified with the Ag content, which thereby enhanced the electric field, that facilitated electron-hole pair separation resulting into increased absorption of light in the visible range [38].

Photocatalytic Activity

The basic mechanism of TiO_2 photocatalysis is the photoinduced generation of electron-hole pairs on the surface of TiO_2 crystal.

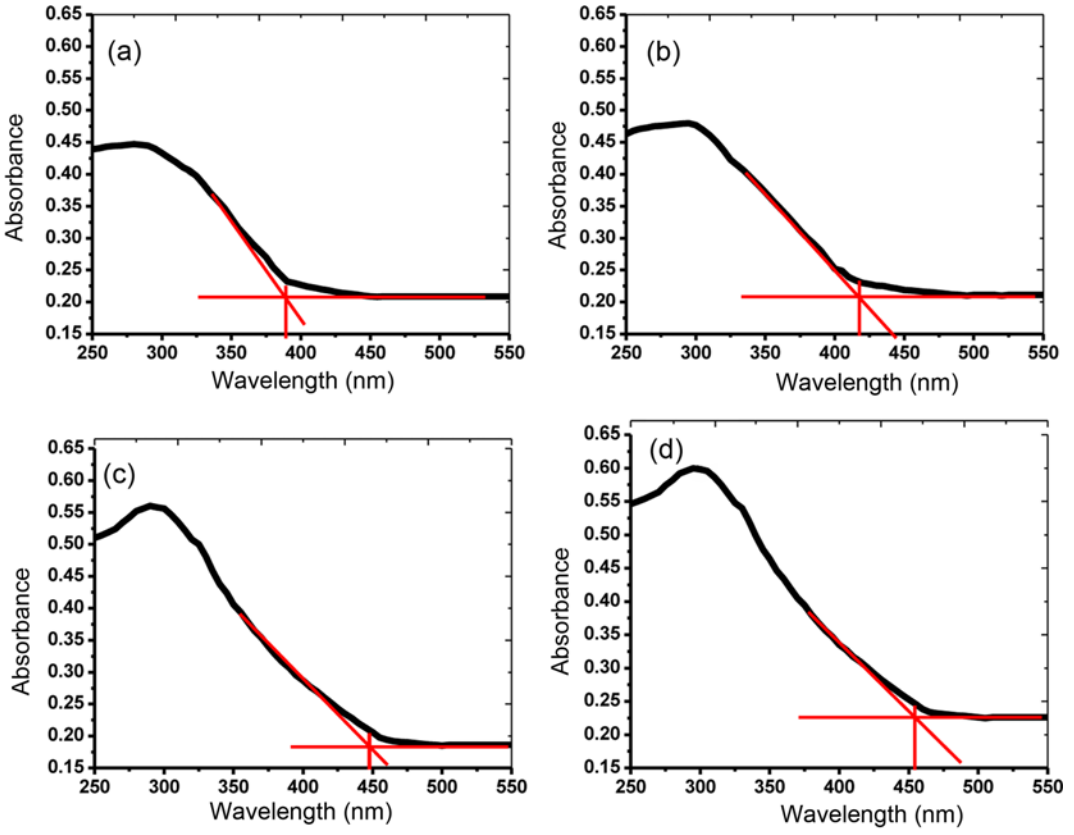

Figure 6. UV-vis absorption spectra of electrospun nanofibers; (a) pristine TiO_2, (b) 2.5 wt%, (c) 5.0 wt%, and (d) 7.5 wt% Ag-loaded TiO_2.

$$TiO_2 + h\nu \longrightarrow e^-_{CB} + h^+_{VB} \quad (5)$$

Electron-hole recombination is expected to occur at this point, releasing energy as heat [39]. However, if the electrons and/or holes transfer to the surface of the crystal, they can participate in various oxidation or reduction reactions with species adsorbed to the surface of catalyst, such as oxygen, water, organic molecules and so on $^{\bullet}OH$ radicals are produced through water molecules or OH^- ions being trapped in the holes [40].

$$H_2O + h^+_{VB} \longrightarrow {}^{\bullet}OH + H^+ \quad (6)$$

$$OH^- + h^+_{VB} \longrightarrow {}^{\bullet}OH \quad (7)$$

$$O_2 + e^-_{CB} \longrightarrow O_2^{\bullet -} \quad (8)$$

$^{\bullet}OH$ and $O_2^{\bullet -}$ are considered to be the significant reactive oxygen species (ROS) and directly oxidize MB dye in the bulk solution [23].

$$MB + {}^{\bullet}OH \longrightarrow \text{decolorization product} \quad (9)$$

$$MB + O_2^{\bullet -} \longrightarrow \text{decolorization product} \quad (10)$$

Figure 7 shows the color variations observed in MB concentration with the interaction of each type of nanofibers as a function of irradiation time during the UV illumination of liquid suspension. In case of Ag-loaded TiO_2 nanofibers, photocatalytic decolorization of MB has been observed to increase as a function of Ag loading, which is attributed to presence of Ag nanoparticles on the outer surfaces of TiO_2 nanofibers. The presence of Ag effectively captured the photo-induced electrons and holes, which were quickly transferred to the oxygen adsorbed on the surfaces of TiO_2 nanofibers. The amount of hydroxyl radicals is also believed to increase on the surfaces of Ag-loaded nanofibers. These characteristics of Ag-loaded TiO_2 nanofibers have remarkably improved their photocatalytic performance [41]. Figure 8 shows UV-visible absorption spectra of MB treated with the pristine and Ag-loaded TiO_2 nanofibers as a function of UV illumination time. From the absorbance measured at λ=664 nm, the corresponding dye concentrations were calculated using the calibration curve. Plots of absorbance versus irradiation time and C/C_0 versus irradiation time for photocatalytic decolorization of MB are given in Figure 9. The kinetics study shows the straight lines with linear regression coefficients (R^2) that are obtained by plotting ln (C_0/C) versus irradiation time (t), which indicates that the kinetics of the photocatalytic decolourization of MB by both pristine and Ag loaded TiO_2 fitted to the Langmuir-Hinshelwood model, as given in Figure 10 [23].

The values of rate of reaction, first-order rate constant and efficiency of photocatalytic decolorization of MB are given

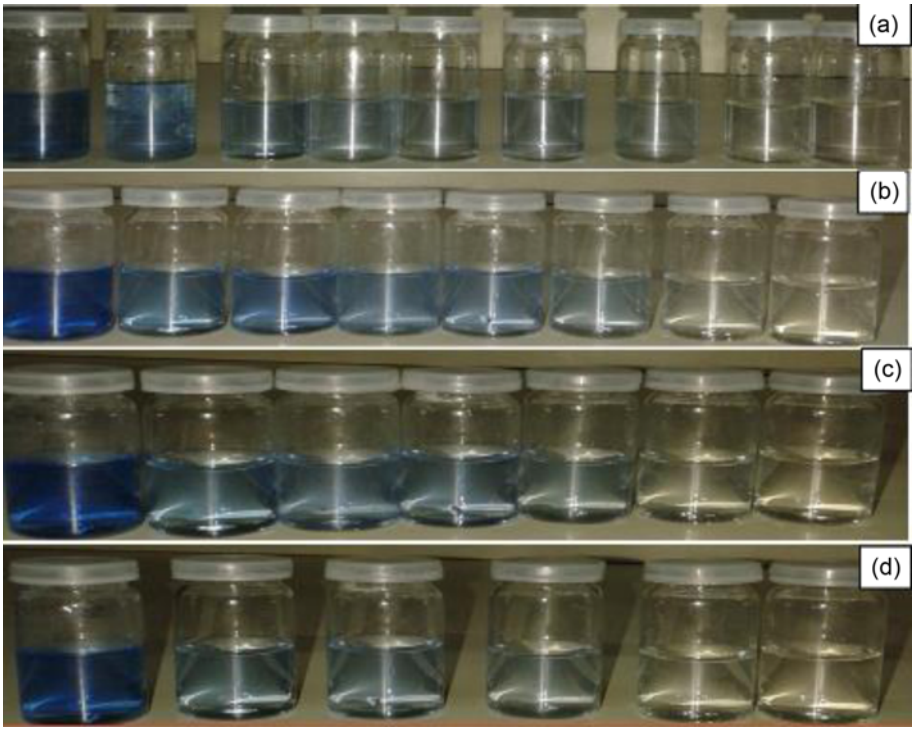

Figure 7. Decolorization of MB treated with electrospun nanofibers used as catalyst by UV irradiation time; (a) pristine TiO_2, (b) 2.5 wt%, (c) 5.0 wt%, and (d) 7.5 wt% Ag-loaded TiO_2.

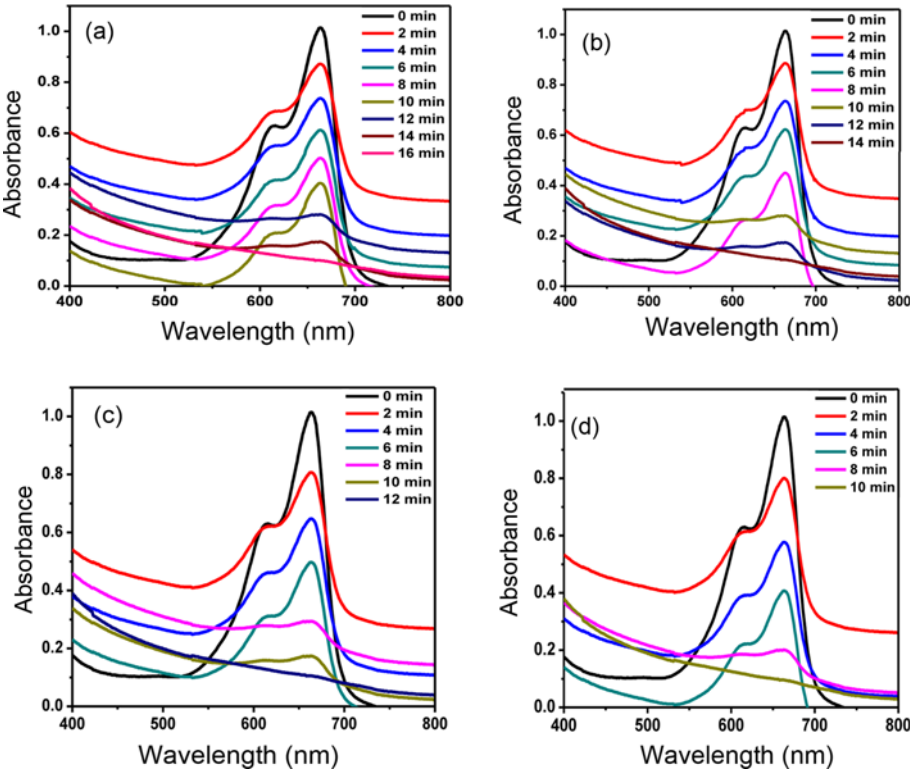

Figure 8. UV-vis spectral changes of MB treated with electrospun nanofibers used as catalyst UV irradiation time; (a) pristine TiO_2, (b) 2.5 wt%, (c) 5.0 wt%, and (d) 7.5 wt% Ag-loaded TiO_2.

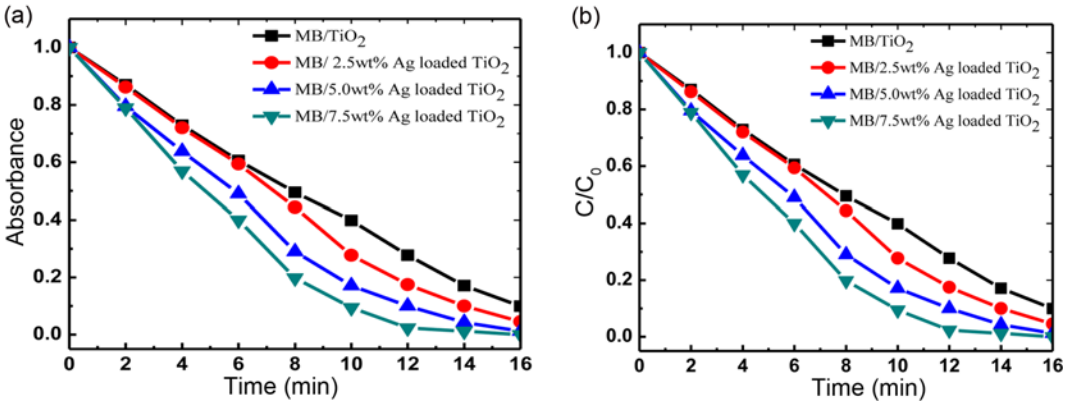

Figure 9. Plots of absorbance versus time (a), C/C_0 versus irradiation time (b) for photocatalytic decolorization of MB.

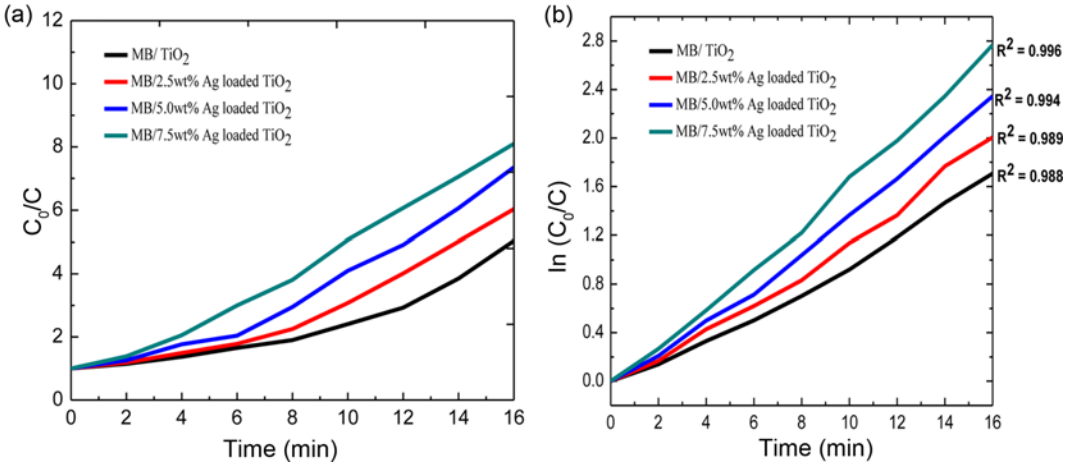

Figure 10. Plots of pseudo-first-order model of photocatalytic decolorization of pristine and Ag loaded TiO_2 nanofibers (a), C_0/C versus irradiation time (b) $\ln(C_0/C)$ versus irradiation time.

Table 1. Cut off wavelength (nm), energy band gap (eV), reaction rate, rate constant of first order reaction, removal efficiency of MB and linear regeression coefficient in the presence of pristine and Ag-loaded TiO_2 electrospun nanofibers at MB concentration 10 mg/*l*, solution pH 6.3 and room temperature

Material	Cutoff wavelength (nm) λ	Energy band gap (eV) $E=hc/\lambda$	Reaction rate (mg/min) $r=dC/dt$	First-order rate constant (k) (min^{-1}) $k=(1/t)\ln(C_0/C)$	Removal efficiency (%) $(C_0-C_t/C_0)\times100$	Linear regeression coefficient (R^2)
TiO_2 nanofibers	389	3.18	0.0567	0.1439	60	0.988
2.5 wt.% Ag-loaded TiO_2 nanofibers	417	2.97	0.0648	0.1608	72	0.989
5.0 wt.% Ag-loaded TiO_2 nanofibers	449	2.76	0.0756	0.1876	83	0.994
7.5 wt.% Ag-loaded TiO_2 nanofibers	454	2.73	0.0918	0.2251	90.5	0.996

in Table 1. From these results, it is observed that decolorization rate and removal efficiency have increased with the rising contents of Ag in these nanofibers. The rationale attributed to such kind of behavior of nanofibers is the reduction in the phase transformation temperature with increasing Ag-loading, as well as rise in the amount of A-phase crystallinity [42]. The mean diameter of Ag-loaded TiO_2 nanofibers is observed to be smaller than the pristine while the crystallites' size of A-phase is smaller than the R-phase, eventually having larger surface area. Surface area is an important characteristic of the materials while being studied for their efficiency as catalysts. The photocatalytic activity of nanomaterials is known to be a function of their surface properties; as when surface area increases, the number of active sites also rises. In order to get better photocatalytic decolorization activity, higher surface area of

the catalyst is often desired [11].

Conclusion

The effect of Ag loading and calcination at 500 °C on the crystal structure, phase transformation, morphology, vibrational phonon bands, and chemical compositions of TiO_2 electrospun nanofibers have been investigated and evaluated. Pristine TiO_2 nanofibers have both found to have A and R-phases, while Ag-loaded exhibited predominantly A-phase with excellent crystallinity and surface morphology. The extent of roughness on the outer surfaces of nanofibers has been found to increase with the Ag-loading, which has been attributed to the formation of Ag nanoparticles. The mean diameter and crystallite size of these nanofibers have been found reduced with the rise in Ag-loading. The energy band gap of Ag-loaded nanofibers has been found reduced while absorbance increased due to the SPR of Ag nanoparticles. The photocatalytic decolorization rate constants of pristine TiO_2, as well as, 2.5, 5.0, and 7.5 wt% Ag loaded nanofibers against MB were computed to be 0.1439 min^{-1}, 0.1608 min^{-1}, 0.1876 min^{-1}, 0.2251 min^{-1} respectively. The decolorization efficiency of these nanofibers has been observed to increase from 60 to 90.5 % with the rise in Ag-content. These nanofibers can be used for photocatalytic decolorization of various pollutants and are expected to play an important role in solving environmental pollution challenges due to their relatively high oxidative power, photostability and nontoxicity.

Acknowledgements

The authors would like to acknowledge the technical support extended by Dr. Mazhar Mehmood and Dr. Tariq Yasin, Department of Materials and Metallergy, Pakistan Institute of Engineering and Applied Sciences (PIEAS), Islamabad 45650, Pakistan.

References

1. M. Nabil, M. Abbas, A. Zaini, and Z. Akmar, *International Biodeterioration and Biodegradation*, **102**, 274 (2015).
2. A. H. Jawad, R. A. Rashid, R. M. A. Mahmuod, M. A. M. Ishak, N. N. Kasima, and K. Ismail, *Desalination Water Treat.*, **56**, 1 (2015).
3. A. H. Jawad, R. A. Rashid, M. A. M. Ishak, and L. D. Wilson, *Desalination Water Treat.*, **57**, 1 (2016).
4. A. H. Jawad, N. S. A. Mubarak, M. A. M. Ishak, K. Ismail, and W. I. Nawawi, *J. Taibah Univ. Sci*., **10**, 1 (2015).
5. R. A. Rashid, A. H. Jawad, M. A. M. Ishak, and N. N. Kasim, *Desalination Water Treat.*, **57**, 27226 (2016).
6. J. C. Colmenares, M. A. Aramendía, A. Marinas, J. M. Marinas, and F. J. Urbano, *Appl. Catal. A-Gen.*, **306**, 120 (2006).
7. T. Mihankhah, M. Delnavaz, and N. G. Khaligh, *Int. J. Green Energy*, **15**, 69 (2018).
8. Z. Huang, R. S. Gurney, T. Wang, and D. Liu, *J. Colloid Interface Sci.*, **527**, 107 (2018).
9. L. Song, J. Xiong, Q. Jiang, and P. Du, *Mater. Chem. Phys.*, **142**, 77 (2013).
10. M. B. Suwarnkar, R. S. Dhabbe, and A. N. Kadam, *Ceram. Int.*, **40**, 5489 (2014).
11. Y. F. Li, W. P. Zhang, X. Li, and Y. Yun, *J. Phys. Chem. Solid*, **75**, 86 (2014).
12. R. Kralchevska, M. Milanova, T. Tisler, A. Pintar, G. Tyuliev, and D. Todorovsky, *Mater. Chem. Phys.*, **133**, 1116 (2012).
13. M. M. Viana, N. D. S. Mohallem, D. R. Miquita, and K. Balzuweit, *Appl. Surface Sci.*, **265**, 130 (2013).
14. A. H. Jawad and M. A. Nawi, *Reaction Kinetics Mechanisms and Catalysis*, **106**, 49 (2012).
15. S. A. H. Jawad and M. A. Nawi, *J. Polym. Environ.*, **20**, 817 (2012).
16. A. Ayati, A. Ahmadpour, F. F. Banttari, B. Tanhaei, M. Manttari, and M. Sillanpaa, *Chemosphere*, **107**, 163 (2016).
17. Z. Batool, M. Raffi, M. Zakria, R. I. Shakoor, R. Rashid, M. Mehmood, and M. A. Mirza, *J. Cluster Sci.*, **28**, 1857 (2017).
18. M. A. Nawi, A. H. Jawad, S. Sabar, and W. S. Wan Ngah, *Desalination*, **280**, 288 (2011).
19. A. H. Jawad and M. A. Nawi, *Carbohydr. Polym.*, **90**, 87 (2012).
20. L. Shudan, D. Yihui, and G. Meirong, *Appl. Surface Sci.*, **258**, 8015 (2012).
21. R. Khajavi and M. Abbasipour, *Scientia Iranica F*, 2029 (2012).
22. M. K. Seery, R. George, P. Floris, and S. C. Pillai, *J. Photochem. Photobiol. A: Chem.*, **189**, 258 (2007).
23. H. Jawad, N. S. Abdul Mubarak, M. A. Mohd Ishak, K. Ismail, and W. I. Nawawi, *J. Taibah Univ. Sci.,* **10**, 352 (2016).
24. G. Hongyu, W. Xiaohong, G. Yihang, and S. Changlu, *Appl. Surface Sci.*, **280**, 720 (2013).
25. W. Chang, F. Xu, X. Mu, L. Ji, G. Ma, and J. Nie, *Mater. Res. Bull.,* **48**, 2661 (2013).
26. H. E. Chao, Y. U. Yun, H. U. Xingfang, and A. Larbot, *J. Eur. Ceram. Soc.*, **23**, 1457 (2003).
27. J. Y. Park, K. J. Hwang, and J. W. Lee, *J. Mater. Sci.*, **46**, 7240 (2011).
28. S. M. Elahi, A. Taghizadeh, A. Hadizadeh, and L. Dejam, *Int. J. Thin Films Sci. Technol.*, **3**, 13 (2014).
29. M. A. Behnajady, N. Modirshahla, M. Shokri, and B. Rad, *Global NEST J.*, **10**, 1 (2008).
30. M. S. P. Francisco and V. R. Mastelaro, *Chem. Mater.*, **14**, 2514 (2002).
31. M. Suwarnkar, R. Dhabbe, A. Kadam, and K. Garadkar, *Ceram. Int.*, **40**, 5489 (2014).
32. D. J. Reidy, J. D. Holmes, and M. A. Morris, *J. Eur. Ceram. Soc.*, **26**, 1527 (2006).

33. A. N. Murashkevich, A. S. Lavitskaya, T. I. Barannikova, and I. M. Zharskii, *J. Appl. Spectroscopy*, **75**, 730 (2008).
34. X. Feng, X. Wang, X. Chen, and Y. Yue, *Acta Mater.*, **59**, 1934 (2011).
35. S. Vlassov, B. Polyakov, M Vahtrus, M. Mets, M. Antsov, R. Saar, and L. Dorogin, *Mater. Charact.*, **100**, 98 (2015).
36. J. Zhang, M. Li, Z. Feng, and J. Chen, *J. Phys. Chem. B*, **110**, 927 (2006).
37. M. Hoffman, S. Martin, W. Choi, and D. Bahnemann, *Chem. Rev.*, **95**, 69 (1995).
38. G. A. Martinez-Castanon, M. G. Sanchez-Loredo, and H. J. Dorantes, *Mater. Lett.*, **59**, 529 (2005).
39. C. Fernández-Rodríguez and J. M. Dona-Rodríguez, *Appl. Catal. B: Environ.*, **125**, 383 (2012).
40. A. H. Jawad, A. F. M. Alkarkhi, and N. S. Abdul Mubarak, *Desalinaton Water Treat.,* **56**, 161 (2015).
41. A. Vohra, D. Y A. Goswami, D. A. Deshpande, and S. S. Block, *Appl. Catal. B: Environ.,* **65**, 57 (2006).
42. J. C. McEvoy and Z. Zhang, *J. Photochem. Photobiol. C: Photochem. Rev.,* **19**, 62 (2014).